Kinetic and equilibrium factors affecting saturation of chromium oxide in soda-silicate melts

Hichem Khedim, Sandra Abdelouhab, Renaud Podor, C. Rapin, Michel Vilasi, Pierre-Jean Panteix, Michael Toplis, François Faure

Kinetic and equilibrium factors affecting saturation of chromium oxide in soda-silicate melts

Hichem Khedim[1], Sandra Abdelouhab[1], Renaud Podor[1,2], Christophe Rapin[1], Michel Vilasi[1], Pierre-Jean. Panteix[1], Michael Toplis[3] and François Faure[4]

[1]Institut Jean Lamour (UMR 7198) – Département CP2S – Equipe 206, Faculté des Sciences et Techniques, Nancy Université, Boulevard des Aiguillettes, B.P. 70239, 54506 Vandoeuvre lès Nancy CEDEX ; France

[2]Institut de Chimie Séparative de Marcoule, UMR 5257, Site de Marcoule, BP 17171, 30207 Bagnols sur Cèze CEDEX, France

[3]DTP (UMR 5562), Observatoire Midi-Pyrénées, 14 Avenue Edouard Belin, 31400 Toulouse, France

[4]Centre de Recherches Pétrographiques et Géochimiques, UPR 2300, 15 rue Notre Dame des Pauvres, 54501 Vandoeuvre lès Nancy France, France

Abstract

Factors controlling the rate at which chromium oxide reaches saturation in Na_2O-x SiO_2 liquids have been studied as a function of melt composition and oxygen fugacity. Under an oxidising atmosphere, liquid Na_2CrO_4 or Cr_2O_3 crystals can be in equilibrium with soda-silicate

melts, depending on the concentration of sodium in the studied system. Under reducing conditions, $NaCrSi_2O_6$ is stabilized in silica-rich melts when T is lower than 1160°C, while Cr_2O_3 is in equilibrium with the sodium-rich melts when T is above 1160°C. The chromium oxide (Cr_2O_3) to pyroxene ($NaCrSi_2O_6$) transformation is described in terms of the time required to attain chemical and textural equilibrium. Na_2CrO_4, $NaCrSi_2O_6$ and Cr_2O_3 phase stability domains are reported as well as the Na_2O-SiO_2-Cr_2O_3 phase diagram in the studied temperature and fO_2 range.

Keywords: glass melts; chromium oxide; solubility; kinetic

Introduction

Most of the metallic alloys used in the glass making industry are chromia (Cr_2O_3) – forming superalloys [1,2]. However, despite the fact that chromia exhibits low solubility in molten glass even at high temperature, there is a general lack of experimental data concerning the factors that affect chromia solubility in molten glasses. This state of art has stimulated specific studies of Cr_2O_3 solubility in the Na_2O-$xSiO_2$ system as a function of temperature (1000-1300°C), glass composition (x=1.5 to 4), partial pressure of oxygen (10^{-18} atm < fO_2 < 0.20 atm) and the addition of other oxides containing network-forming and/or network-modifying cations (B_2O_3, Al_2O_3 or CaO) [3-7]. One of the principal results of these recent studies is that the attainment of thermodynamic equilibrium involves a large number of reactions between numerous chromium-bearing species in mineral, liquid and gaseous phases, even in a compositionally simple system [5-7]. This complex situation is due to the fact that chromium can exhibit several oxidation states depending on temperature, oxygen fugacity fO_2, and melt composition. For example, in air, Cr^{III} and/or Cr^{VI} species dominate, while under more reducing conditions Cr^{II} may coexist with Cr^{III} [5-7].

The work presented here considers the mechanisms leading to a thermodynamic equilibrium from a simple initial scenario of crystalline Cr_2O_3 placed in contact with liquids in the Na_2O-$xSiO_2$ system. In detail, the aim is to quantify the kinetics of individual reactions (under various fO_2 conditions), to identify which of these processes may be rate-limiting, and to constrain the time-scale for attaining thermodynamic equilibrium. The reactions that may occur are presented in Figure 1 [5-7]. An essential step towards equilibrium involves the dissolution of crystalline Cr_2O_3, to form Cr^{III} oxy-anions in the liquid (equation 1). Equation 1 is written involving oxygen-species of the melt ($O^{2-}_{(melt)}$) to highlight the fact that melt basicity influences the behaviour of chromium in this system.

$$\tfrac{1}{2}Cr_2O_{3\,(crystal)} + xO^{2-}_{(melt)} \Leftrightarrow Cr^{III}O_{x+3/2}{}^{2x-}_{(melt)} \qquad \textbf{Equation 1}$$

In the simplest case these Cr^{III}-bearing anions ($Cr^{III}O_{x+3/2}{}^{2x-}_{(melt)}$) may be stable. Alternatively, depending on oxygen fugacity, reduction to Cr^{II}-bearing species, or oxidation to Cr^{VI}-bearing species may occur in the liquid (described by equations 2 and 3 respectively):

$$2Cr^{III}O_{x+3/2}{}^{2x-}_{(melt)} + (2y - 2x - 2)O^{2-}_{(melt)} \Leftrightarrow 2Cr^{II}O_y{}^{(2y-2)-}_{(melt)} + 1/2O_{2\,(g)} \qquad \textbf{Equation 2}$$

$$2Cr^{III}O_{x+3/2}{}^{2x-}_{(melt)} + 3/2O_{2\,(g)} + (2y\text{-}2x - 6)O^{2-}_{(melt)} \Leftrightarrow 2Cr^{VI}O_y{}^{(2y-6)-}_{(melt)} \qquad \textbf{Equation 3}$$

The reduction reaction (Eq 2) can be neglected in oxidising atmospheres such as air, but must be taken into account under more reducing conditions. On the contrary, the oxidation reaction described by Eq 3 can be neglected in a strongly reducing atmosphere. It is also worth of note that if oxygen fugacity conditions are highly reducing or highly oxidising, crystalline Cr_2O_3 may no longer be the stable phase in equilibrium with the liquid and other Cr-bearing phases may precipitate. Furthermore, under oxidising conditions the behaviour of chromium is complicated by the volatility of Cr^{VI} (principally in the form of $CrO_{3(g)}$ [8]. This is particularly true for Na_2O-rich melts of the system Na_2O-$xSiO_2$ in air, for which Cr^{VI} species are known to be stable [9,10]. Formation of $CrO_{3(gas)}$ may occur from Cr^{VI} oxy-anions in the liquid (equation 4), or through

direct oxidation/volatilisation of unreacted Cr_2O_3 crystals that are in contact with the surrounding atmosphere (equation 5). Both of these equilibria are considered in this study because CrO_3 formation from Cr_2O_3 is known to occur in air when T>1000°C [11].

$$2CrO_y^{(2y-6)-}_{(melt)} + 6O^{2-}_{(melt)} = 2CrO_{3\,(gas)} + 2yO^{2-}_{(melt)} \quad \textbf{Equation 4}$$

$$Cr_2O_{3\,(crystal)} + 3/2O_{2\,(gas)} = 2CrO_{3\,(gas)} \quad \textbf{Equation 5}$$

From a kinetic point of view, a constant concentration of chromium in the liquid phase will only be possible if the rate of Cr_2O_3 crystal dissolution (equation 1), and the rates of reduction or oxidation (equations 2 and 3), are rapid compared to the volatilisation of CrO_3 (equations 4 and/or 5). Furthermore, if a phase different from Cr_2O_3 is stable in the liquidus then the crystallisation of this new phase may also affect achievement of the equilibrium state. In this study, the kinetics of individual dissolution and volatilisation reactions described above (equations 1 and 5) are quantified in the Na_2O-$xSiO_2$ system. The limits of the phase field of Cr_2O_3 are also considered, and alternative saturating phases and their stability fields are identified. The work is mainly experimental, but it also involves quantification of the liquid and solid compositions, as well as the relative proportions of the present phases, as detailed below.

I Experimental procedure

I.1. Synthesis of glasses

Several glasses were prepared for the Na_2O-$xSiO_2$ system with $1.5 \leq x \leq 4.0$. 300g of each Cr-free glass were synthesised from mixtures of reagent Na_2CO_3 (Aldrich, 99.5%) and SiO_2 (Aldrich, 99.9%). After weighing, the powders were mixed in a RETSCH® agate mortar for 15 minutes using a rotation speed of about 60 rpm. The subsequent mixture was then placed in a platinum crucible and held for 2 hours at 1200°C, then 2 hours at 1400°C and finally 24 hours at 1100°C. The time spent at 1400°C was kept relatively short in order to limit the loss of Na_2O.

The chemical composition of some Cr-free glass was determined using Inductively Coupled Plasma Atomic Emission Spectroscopy (ICP-AES). These results (Table 1) show a small difference between the nominal Na / Si and those determined by ICP-AES. This offset does not exceed 3 relative % and can be attributed to a small extent of sodium volatilisation during the synthesis of the glass at high temperature. Chromium oxide was then added to each glass as crystalline Cr_2O_3 (Alfa Aesar, 99%). The mixtures were thoroughly mixed by grinding in an agate mortar.

I.2. *Experimental methods*

The experiments were performed in a 1750°C Nabertherm® muffle furnace. A Pt - 10%Rh thermocouple was systematically introduced into the furnace near the sample in order to measure the temperature. Two different experimental procedures were employed.

For the first procedure, approximately 100 mg of the glass + Cr_2O_3 mixture was pressed onto platinum wire loops using polyvinyl alcohol as a binder and pre-heated for 2 minutes at T=1000°C. The diameters for the Pt-wire and the loops are approximately 0.2 mm and 2-3 mm respectively. Typically, six samples prepared in this way were hung together in the furnace, each sample being attached to an independent 1mm diameter Pt wire. The gas in the tube furnace is air, and individual wire loops were removed from the furnace after different durations.

The second procedure was designed for working under reducing conditions [12]. Approximately 100 mg of glass + Cr_2O_3 mixture was placed in a Pt-container, introduced into a silica tube which was sealed under secondary vacuum and then heated at the desired temperature in a muffle furnace. In order to limit Na_2O volatilisation, a sample of the same glass composition was added in the reactor, buffering the partial pressure of Na_2O. The oxygen fugacity in the reactor was controlled by the use of different oxide/metal solid buffers. After the required run

duration, which is depending on temperature and glass composition, the silica tubes were removed from the furnace and quenched in cold water.

I.3. *Sample preparation and analysis*

Quenched samples were embedded in epoxy resin and then polished to 1 µm using anhydrous ethanol as a lubricant. The polished sections were then analysed using a fully automated CAMECA SX 100 electron microprobe with 5 Wavelength Dispersion Spectrometers (WDS). The elements analysed were Na, Si and Cr. The concentration of oxygen was calculated by stoichiometry assuming that the valence states of the cations are 1, 4 and 3 respectively. The standards used were $NaAlSi_3O_8$ for Na and Si, and Cr_2O_3 for Cr. The values of accelerating voltage and beam current were chosen depending on the distribution of Cr_2O_3 crystals in the glass. When the Cr_2O_3 crystals were smaller than 2 µm and the maximum distance between two crystals was less than 25 µm, the electron beam conditions were 10kV and 5nA. Because of the presence of abundant crystals of Cr_2O_3 which limited the size of glass pools, an incident-beam diameter of 5 µm was used. When the Cr_2O_3 crystals were larger than 2 µm and the maximum distance between two crystals was greater than 25 µm, the electron beam conditions are 25kV and 10nA. The incident beam diameter was 12 µm. The analysis conditions (accelerating voltage, beam current, counting times on peaks and backgrounds, average volume analysed) are reported in Table 2. In both cases, the three elements were analysed on three distinct wavelength dispersion spectrometers at the same time.

Comparative results of analyses performed on a Na_2O - $2SiO_2$ glass doped with 1 wt% Cr_2O_3 using both electron beam conditions are reported in Table 2 and illustrated in Figure 2. These results indicate that the analyses performed with the second program are much more precise than those performed at lower acceleration voltage. Furthermore, the dispersion of the values around the mean is higher when the analyses are obtained using a low acceleration

voltage. However, even in this case, electron microprobe measurements of the starting glasses are found to be systematically depleted in sodium relative to the values determined by ICP-AES (Table 1), implying some volatilisation of sodium under the electron beam at these conditions (the Na_2O depletion is even more intense when the P1 program is used). However, the magnitude of this effect is limited and never exceeds 5 relative percent. Thus, a large beam size and a high voltage conditions (P2 program) have been used whenever possible. Unless otherwise stated, these are the analysis conditions for measurements shown in Table 2 such that all analyses are comparable.

I.4. Determination of the volume (and mass) fraction of Cr_2O_3 crystals in a glass pellet using image analysis

The quantification of the Cr loss by CrO_3 volatilisation requires the determination of the bulk-Cr content of the samples after heat treatment. For this purpose, quantification of the relative proportions of residual Cr_2O_3 crystals and coexisting glass is required. To quantify the volume (or mass) fraction of Cr_2O_3 crystals, digital photographs of the polished sections surface of the sample were taken under reflected light using an Olympus Vanox AHMT optical microscope. These images, in which glass is clearly distinguished from crystals, were treated using the AnalySIS software [13], which allows the determination of the relative surface areas of glass and Cr_2O_3. These values were then converted into relative mass proportions using the referenced density values (ρ) of glass and crystals [14,15]. The sample was then re-polished in order to remove approximately 100µm of thickness and another set of images were recorded and analysed. These procedures were repeated until the whole sample was investigated. The bulk Cr_2O_3 weight percentage of the samples was determined using the following equation:

$$\%wtCr_2O_3(crystal) = \frac{\sum_{i=1}^{n} \%Cr_2O_3(surface) \times e \times \rho(Cr_2O_3)}{\left[\left(\sum_{i=1}^{n} \%Cr_2O_3(surface) \times e \times \rho(Cr_2O_3)\right) + \left(\sum_{i=1}^{n} \%glass(surface) \times e \times \rho(glass)\right)\right]} \times 100$$

Equation 6

With i = 1: first image analysis , i = n : last image analysis, e : thickness loss of the sample

II. Results

II.1 Volatilisation of Cr(VI) dissolved in the glass melt

Before considering how crystalline Cr_2O_3 dissolves in sodium-silicate melts (equations 1 to 3), the loss rates of Cr^{VI} species are first considered (equations 4 and 5). In order to quantify the rate of the reaction 4, 10g of Na_2O-$2SiO_2$ glass doped with 1 wt% Cr_2O_3 was prepared from a mixture of Na_2O-$2SiO_2$ glass and Cr_2O_3 crystals, heated at 1100°C for 24h in air. This concentration of Cr_2O_3 being below the saturation level [5-7], no crystalline Cr_2O_3 should be present in the melt. The glass composition was determined by EPMA (Table 1), and the mass fraction of Cr_2O_3 in the glass was found to be 0.93 ± 0.04. Observation under the optical microscope confirmed the absence of crystalline Cr_2O_3. This starting material was then used for subsequent time-series experiments. The obtained glass was yellow, indicating the presence of Cr^{VI} [5-7].

150 mg beads of this glass were suspended on a Pt wire and heated at 997°C, 1107°C, 1207°C and 1310°C for run durations ranging from 10 to 120 minutes. The concentration of Cr_2O_3 after the heat treatment was quantified by EPMA from the core to the rim of each sample. These measurements indicate that there is no chromium concentration gradient between the edge and the centre of the samples. On the other hand the average values of Cr_2O_3 are decreasing as time increases. This result is interpreted in terms of loss of Cr^{VI} over time, while the lack of an internal concentration gradient implies that volatilisation is not limited by the diffusion of chromium in the glass.

In detail, the mass fraction of Cr_2O_3 remaining in the melt decreases with increasing temperature and run duration (Table 3; Figure 3). Assuming that loss of Cr^{VI} occurs through a surface controlled process, it may be shown that the volatilisation rate at a constant temperature can be derived from the variation of C/C_0 as a function of time, where C is the concentration of Cr in the liquid at the considered time, and Co is the initial concentration. The variation of C/Co is found to be linear as a function of time at constant temperature, allowing the definition of V_R (the volatilisation rate of Cr^{VI}), at the measured temperature (Table 3). As expected, the volatilisation is faster at higher temperature. The kinetics of Cr volatilisation is totally different from the alkali-metal oxide (Na_2O or K_2O) volatilisation. Indeed, in the case of alkalis, volatilisation curves exhibit logarithmic variations with time exposure [16-17], while Cr volatilisation is linear with time.

Furthermore, when $\ln(V_R)$ is plotted as a function of inverse temperature, an Arrhenian temperature dependence is found (Figure 4). From this correlation it is possible to quantify the activation energy for the volatilisation of Cr^{VI} species dissolved in Na_2O-$2SiO_2$ liquid (equation 7):

$$\ln V_R = C - \frac{E}{R} \times \left(\frac{1}{T} \right) \qquad \textbf{Equation 7}$$

where C is a constant, R is the ideal gas constant, T is the absolute temperature, and E is the activation energy. The value of E derived from this set of data is 108 $kJ.mol^{-1}$.

II.2 Volatilisation of CrO_3 from Cr_2O_3 crystals

In the absence of melt, the formation and volatilisation of CrO_3 from Cr_2O_3 crystals (equation 5), has been investigated by Stearns [18]. He showed that this reaction can be neglected when the temperature is lower than 1000°C, but in the temperature range of this work, this

reaction must be taken into account. To confirm the influence of relation 5 and to quantify its effect, an additional experiment has been performed using Na_2O-1.5SiO_2 + 40wt% Cr_2O_3 mixture heated in air at 1300°C for 120 minutes. This amount of Cr_2O_3 is much higher than the equilibrium content of 8.15 wt% Cr_2O_3 for this composition at T=1300°C [3]. The volatility of chromium in this experiment has been quantified by performing a mass balance calculation of the heat-treated sample. For this purpose the remaining Cr_2O_3 crystals has been quantified from 3D reconstruction of the sample (part I.4), and the liquid composition has been determined by EPMA. The mass of Cr_2O_3 lost from the sample may be determined using the following equation:

$$wt\%Cr_2O_{3\,(volatilised)} = wt\%Cr_2O_{3\,(intial\ crystal)} - (wt\%Cr_2O_{3\,(melt)} + wt\%Cr_2O_{3\,(final\ crystal)}) \quad \textbf{Equation 8}$$

where:

wt% $Cr_2O_{3(initial\ crystal)}$: Initial Cr_2O_3 content in the glass before the heat treatment = 40%

wt% $Cr_2O_{3(melt)}$: Final Cr_2O_3 content dissolved in the glass after the heat treatment = 10%

wt% $Cr_2O_{3(final\ crystal)}$: Final Cr_2O_3 content in the crystal after the heat treatment = 16%

Using these values, a loss of 14 wt% $Cr_2O_{3(volatilised)}$ is obtained, resulting from both direct volatilisation of Cr_2O_3 crystal as well as volatilisation of Cr^{VI} species dissolved in the liquid (the effects of reaction 4 and 5 cannot be decoupled). Assuming that the Cr^{VI} volatilisation rate from the Na_2O-1.5SiO_2 liquid is approximately the same as that determined for the Na_2O-2SiO_2 melt, the predicted loss of Cr_2O_3 directly from the liquid after 2 hours is approximately 0.6 wt%. It can be concluded that the principal contribution to chromium loss during this experiment was the volatilisation of crystalline Cr_2O_3 (reaction 5) rather than loss from the liquid (reaction 4). This result implies that a sufficient excess of crystalline Cr_2O_3 must be added to the initial mixture when quantifying the equilibrium concentration of chromium in a Cr_2O_3 saturated liquid.

II.3 Dissolution kinetics of Cr_2O_3 under oxidising conditions

As noted above, in the Na_2O-$xSiO_2$ system, the dissolution of crystalline Cr_2O_3 can produce Cr(III) and/or Cr(VI) in the liquid when the system is in equilibrium with an oxidising atmosphere such as air (equations 1 and 3). In this section the experimental dissolution of crystalline Cr_2O_3 into sodium-silicate liquids is described as a function of temperature under such conditions. Liquids of Na_2O-$1.5SiO_2$, Na_2O-$2SiO_2$, Na_2O-$3.5SiO_2$ and Na_2O-$4SiO_2$ compositions, to which 5 to 20 wt% Cr_2O_3 have been added, were studied. Experiments were performed on glass beads placed directly in the furnace as described above. Identification of the presence of Cr(VI) species was simplified by the fact that such species impart a yellow colour to the glass. Optical and SEM observations of heat treated samples show that for a short heat treatment, the external part of samples contains higher amounts of Cr(VI) and lower amounts of residual crystalline Cr_2O_3 compared to the central part of the sample (Figure 5). For this case, EPMA analyses show significant differences in total chromium content (corresponding to the sum of Cr(III) and Cr(VI)) between the core and rim, sample rims being systematically enriched in dissolved chromium in comparison to the core (Figure 6). With increasing time, the optically visible limit of the oxidised zone migrates towards the centre of the sample. In terms of liquid chemistry, the Cr-content of the sample rim is more or less constant, while the Cr-content of the core increases, finally reaching values observed at the sample rim.

In detail, the time required for core and rim compositions to converge depends on the liquid composition and temperature, as discussed below, while in certain cases chromium concentration decreases at the sample rim for long run duration.

Based upon these results the following sequence of events can be proposed:

- Upon heating above the glass transition, the dissolution of Cr_2O_3 crystals occurs througout the sample, producing Cr^{III} in the liquid.

- A fraction of the dissolved Cr^{III} species is subsequently oxidised, but this reaction (equation 3) is limited by the availability of oxygen, initially introduced at the surface of the sample and then transported by diffusion to the bulk.
- During this stage preferential loss of CrO_3 through volatilisation leads to more rapid elimination of residual Cr_2O_3 grains in parts of the liquid dominated by Cr^{VI} species.
- Once the limit of the oxidised zone has moved through the whole sample, an approach to equilibrium may be reached, as illustrated by cases where the mole fractions of total chromium are equal at the rim and at the core of the sample (Figure 6).
- If the heat treatment of the sample is prolonged, the continuous loss of Cr^{VI} species at the edge of the sample may lead to a decrease of the total chromium content of the liquid, by a combination of the mechanisms described in equations 4 and 5.

As noted above, the comparison of data for different liquids shows that the time to reach a state of equilibrium (convergence of core and rim compositions) depends on the liquid composition and temperature; For example, as illustrated in Figure 6, equilibrium is reached earlier in the Na_2O-$2SiO_2$ melt than in the Na_2O-$4SiO_2$ melt, even if the final total chromium content is lower in Na_2O-$4SiO_2$ compared to Na_2O-$2SiO_2$. This behaviour may be observed due to the rate of oxygen diffusion. For example, from a qualitative point of view, Na_2O-$4SiO_2$ liquid is more polymerised than Na_2O-$2SiO_2$, such that oxygen diffusion in the former composition is slower, thus requiring more time to reach an equilibrium state in terms of Cr concentration. This idea may be tested in a more quantitative way, given that the diffusion coefficent of oxygen is known to be proportional to shear viscosity [19,20]. Indeed, when the time required to reach equilibrium is considered as a function of the shear viscosity of the liquid (estimated from literature data for binary sodium silicates [21-23]), a very good correlation is observed (Figure 7), supporting the idea that the time required to reach equilibrium is indeed controlled by oxygen diffusion. This correlation seems to word as for a given melt composition at known temperature

(i.e. a given liquid viscosity), the time to reach equilibrium may be determined from Figure 7 once a sample geometry correction has been made (all samples here are considered as glass pellets of 5mm diameter).

One final point of note is that electron micro-probe analyses of crystalline phases in these experiments showed that small drops of Na_2CrO_4 were observed on the platinum wire directly in contact with the silicate melt when $x \leq 2.5$. This compound is a liquid at the experimental temperature, but is inferred to be the liquidus phase (rather than Cr_2O_3) for sodium-rich melts under oxidising conditions. For compositions with $x>2.5$, the stability of Cr_2O_3 depends on temperature, as detailed below.

II.4 Dissolution kinetics of Cr_2O_3 under reducing conditions

A similar procedure has been performed under reducing conditions in order to determine the effect of fO_2 on the kinetics of dissolution. Under low fO_2, oxidation of Cr^{III} to Cr^{VI} and associated volatility are not expected. The formation of Cr^{II} species may be predominant (eq. 2). For these experiments, the temperature is found to play a major role, and the results above and below 1160°C are distinguished.

II.4.1 T > 1160°C

When temperature is higher than 1160°C at low oxygen fugacity, the dissolution of Cr_2O_3 is often accompanied by a change of melt color from green to blue due to the presence of Cr^{II} species. Crystalline textures and dissolved Cr content are reported in Figure 8 as a function of run duration. The dissolution process is found to be accompanied by an aggregation of Cr_2O_3 crystals and the formation of extensive zones enriched in dissolved Cr. In these conditions, the time necessary to reach equilibrium was established to be no longer than 16 hours. Similar behaviour is observed for all the compositions.

II.4.2 T<1160°C

In the temperature range from 1100 to 1160°C, under reducing conditions, a significant difference in behaviour is observed between silica-rich and silica-poor liquids. For silica-poor liquids (Na_2O-1.5SiO_2 and Na_2O-2.5SiO_2), Cr_2O_3 is the only crystalline product that is in equilibrium with the melt. In the case of Na_2O-2SiO_2 melt, under a Ni/NiO buffered atmosphere and T=1100°C (Figure 9), equilibrium is reached in less than 24 hours, and no significant changes are measured in the Na/Si ratio of the melt relative to the initial value.

On the other hand, when the melt composition is silica-rich ($2.5 < x < 5$), and the temperature less than 1160°C, a more complicated behaviour is observed. Several experiments have been performed as a function of temperature, with run durations up to 96 hours. The samples exhibit a variety of features as a function of run duration, which can be discussed as the following points:

1. For a short run durations, a crystal-free zone develops at the melt/gas interface, with extended zone where crystalline Cr_2O_3 is in equilibrium with the melt (Figure 10). During this step the melt contains a relatively high content of dissolved Cr.
2. After a few hours (the exact duration depends on temperature and melt composition, but is generally more than 16 hours) the Cr_2O_3 crystals initially present in the melt (1 to 5 µm in diameter) coalesce to form aggregates, typically 10 to 100µm in diameter. At this time, the precipitation of crystals of $NaCrSi_2O_6$ pyroxene (kosmochlor) is observed. The fact that the crystallisation of pyroxene does not take place immediately may imply that its nucleation is delayed. In this respect, the skeletal shape of pyroxene crystals is consistent with a rapid growth, potentially related to supersaturation. It is noted that the delayed nucleation and rapid growth are typical features of pyroxene crystallisation in both natural and experimental systems [24-27]. Immediately after the appearance of the first pyroxene

crystals, two different zones of the samples which are enriched in crystalline Cr_2O_3 and $NaCrSi_2O_6$ can be distinguished respectively. The Cr concentration of the melt is observed to be significantly lower in the zones rich in pyroxene crystals.

3. With further increase in time, the complete dissolution of Cr_2O_3 and the precipitation of $NaCrSi_2O_6$ throughout the whole sample occur. The pyroxene crystals can be large enough to fall to the bottom of the melt drop. Some of these crystals are even big enough to fall out of the bead. Therefore, under these conditions, it would therefore appear that crystalline Cr_2O_3 is not stable, and that the chromium content of a liquid in equilibrium with pyroxene crystals is lower than that of the same liquid in equilibium with crystalline Cr_2O_3.

The attainment of equilibrium at these conditions was checked by comparing the final Cr solubilities determined by dissolving Cr_2O_3 crystals in Na_2O-3.25SiO_2 melt (undersaturated experiment) or reprecipitating crystals from Cr_2O_3 supersaturated Na_2O-3.25SiO_2 melt (supersaturated experiment) under Ni/NiO buffered atmosphere, at T=1150°C. Final chromium contents are reported in Figure 11 as a function of run duration. Chromia dissolution and precipitation equilibria were reached after 25 hours run duration. No significant changes are measured in the final Na/Si ratio in the melt drops. $NaCrSi_2O_6$ is the only product that is in equilibrium with the Na_2O-3.25SiO_2 melt after 50 hours run duration at this temperature.

II.5 Determination of the transition temperature from Cr_2O_3 to $NaCrSi_2O_6$

The total chromium solubilities determined in Na_2O-3SiO_2 melt are plotted in an Arrhenius diagram, for temperatures in the range from 1100 to 1250°C (Figure 12). The lower temperature domain corresponds to the liquids in equilibrium with $NaCrSi_2O_6$, while the higher

temperature domain corresponds to the liquids in equilibrium with Cr_2O_3. Data from each domain are self-consistent, but there is a clear change in slope of the variation of Cr-content of the liquid between these two domains. The temperature at which the change in slope occurs is interpreted as the transition temperature from the domain in which the melt is in equilibrium with Cr_2O_3 to that in equilibrium with $NaCrSi_2O_6$. As illustrated in Figure 12, this temperature is estimated to be 1160(±15)°C for Na_2O-3SiO_2.

An interesting point to note is that for silica-rich melts at temperature lower than 1160°C, the melt may be in metastable equilibrium with Cr_2O_3 crystals for many hours before the appearance of pyroxene crystals. When the chromium content of these metastable liquid compositions is considered, an excellent agreement with equilibrium values extrapolated from higher temperature is observed (Figure 12). Finally, the reversibility of this reaction has been tested while dissolving pyrochlor crystals in soda-silicate melts at T=1200°C, in Na_2O-3SiO_2 melt. In this case, only Cr_2O_3 crystals are observed to be in equilibrium with the melt after 24 hours run duration.

II.6 Effect of fO_2 and temperature on crystallisation

II.6.1 Decreasing the fO_2

The study of the effect of decreasing the fO_2 on Cr_2O_3 crystallisation in melt has been performed using Na_2O-2SiO_2 melt equilibrated with 3 wt% Cr_2O_3 in air (oxidising conditions), at T=1200°C. At this condition, Cr dissolved in the melt is dominantly in the form of Cr^{VI} species [5-7]. The melt drop was placed in a graphite crucible and heated for 5 minutes at T=1200°C. In this reducing atmosphere, the Cr^{VI} present at the edge of the melt drop is quickly reduced to the 3+ oxidation state. The Cr^{III} content in this part of the melt becomes higher than the Cr_2O_3 solubility limit and results in a rapid precipitation of Cr_2O_3 crystals, as evidenced by the acicular

morphology of these crystals (Figure 13). Moreover, Cr_2O_3 crystals display a preferential orientation that is typical of constrained growth under a compositional or thermal gradient [28].

II.6.2 Decreasing the melt temperature

The effect of a decrease in temperature has also been studied. The Cr^{III} supersaturated melt drops used for reprecipitation experiments were prepared by completely dissolving Cr_2O_3 crystals in Na_2O-3.25SiO_2 melt at T=1250°C, in the presence of a Ni/NiO buffer. Samples were then heated at 1150°C for durations varying from 1 to 49 hours. The quantity and morphology of Cr_2O_3 and pyroxene crystals were systematically determined. The data collected are summarized in Figure 14 and 15. The Cr_2O_3 crystals nucleate very rapidly and the number of nucleus reaches a maximum after 9 hours (Figure 14b). Their platelet-like morphology (Figure 14a) is characteristic of crystals grown from a supersaturated liquid. Subsequently, the Cr_2O_3 crystal density slowly decreases and the mean size of the Cr_2O_3 crystals increases as a function of time, thus indicating grain ripening (Figure 14c).

The total number of $NaCrSi_2O_6$ crystals which have nucleated and grown in the melt (Figure 15a) are much more difficult to determine compared to the Cr_2O_3 grains. Indeed, the pyroxene crystals grow very rapidly (Figure 15b) and, as their density is higher than that of the melt, they sediment to the bottom of the melt drop. They are thus generally concentrated in this part of the sample and their distribution in the sample cross section is not as representative as that of Cr_2O_3. Nevertheless, the data reported in Figure 15b and 15c indicate that the size of these crystals is very large.

III Discussion: stability domains of chromium species and phases diagrams

III.1 Stability domains of Cr-containing solid phases in equilibrium with soda-silicate melts

The compositions of the solid phases that are in equilibrium with the silicate melt strongly depend on melt composition. Three distinct phases have been found to be in equilibrium with the liquid. Their respective stability domains are reported in Figure 16. Liquid Na_2CrO_4 is in equilibrium with Na_2O-rich melt in the high fO_2 domain. The phase stability domain of $NaCrSi_2O_6$ pyroxene covers the Na_2O-poor part of our system, when temperature is lower than 1160°C, irrespective of fO_2. Cr_2O_3 is the stable equilibrium phase in the rest of the (T, x, fO_2) domain.

Data of the literature have only described the presence of Cr_2O_3 in equilibrium with soda-silicate melts [29-32], both during dissolution tests of chromium oxide, and studies of the corrosion of chromium-bearing alloys by molten silicates. In particular, the formation of pyroxene crystals is generally not reached during corrosion experiments performed using chromia-former alloys [33]. The formation of pyroxene crystals at the metal/melt interface was previously reported only once [3,34], but was not explained in details.

III.2 Na_2O-Cr_2O_3-SiO_2 phase diagram

The Na_2O-SiO_2-Cr_2O_3 phase diagram can be established in the Cr_2O_3 and SiO_2-rich domain, under reducing conditions. Two distinct phase diagrams corresponding to the temperature domains T<1160°C and T>1160°C are reported in Figure 17 and 18 respectively.

The low-temperature phase diagram (Figure17) shows the presence of the $NaCrSi_2O_6$ compound, a Na_2O-xSiO_2 liquid phase that is enriched in Cr_2O_3 and three distinct phase domains consisting of:

(a) SiO_2 – Cr_2O_3 – L1

(b) L1 – $NaCrSi_2O_6$ – Cr_2O_3

(c) $NaCrSi_2O_6$ – Cr_2O_3 – L2

The $NaCrSi_2O_6$ compound is not stable in the high-temperature part of the Na_2O-SiO_2-Cr_2O_3 phase diagram (Figure18). Only one-three phased domain, corresponding to the SiO_2 – Cr_2O_3 – L3 equilibrium, still exists when T is higher than 1160°C. In this case, Cr_2O_3 or SiO_2 crystals are in equilibrium with the Na_2O-$xSiO_2$ liquid compositions.

Concluding remarks

The objective of this work is to determine the dissolution kinetics of chromium oxide in soda-silicate melts, in order to determine the times necessary to attain the equilibrium state. Equilibrium values and dissolution mechanisms have consequently been studied, requiring development of a variety of new experimental procedures:

- In order to limit sodium loss through volatilisation and thus maintain a constant glass composition, certain experiments were performed in a reactor, developed in our laboratory [5,12], in which temperature and oxygen fugacity may be independently controlled.
- The analysis conditions for the EPMA have been carefully studied and optimised in order to systematically control glass compositions, and the results of certain EPMA analyses have been compared to those obtained by ICP-AES measurements.
- A specific effort has been made to consider all possible reactions between Cr-bearing species. In detail, chromia dissolution in silicate melts can be described by 5 equations:
    - an acid-base reaction (dissolution to produce Cr^{III} species in the liquid)
    - two redox reactions (oxidation and reduction of dissolved Cr^{III} into Cr^{VI} and Cr^{II} respectively)

- two volatilisation reactions which produce CrO_3 gas. This reaction can be due to (i) the volatilisation of dissolved Cr^{VI}, and/or (ii) the oxidation of crystalline Cr_2O_3. The importance of these reactions has been quantified by specific experiments. It has been shown that they are of negligible importance for temperatures higher than 1000°C.

The principle results obtained may be summarized as follows:

- The time to reach equilibrium mainly depends on temperature and melt composition (*i.e.* viscosity and oxygen diffusivity). Indeed, at fixed temperature, a short equilibration time (a few minutes) can be expected when studying basic melts under oxidising atmospheres, while very long run durations are necessary to reach the thermodynamic equilibrium in silica-rich melts, under reducing conditions.
- The rate limiting effect of oxygen diffusion on the oxidation (or reduction) of chromium is clearly illustrated by the concentric zone of melt drops after short reaction times. In these cases, the differences between the chromium contents in the core and in the rim of the glass drops are important and are attributed to differences in the extent of the oxidation (or reduction) reaction.
- The main parameter that controls and limits the kinetics of chromium dissolution in soda silicate melts is the oxygen diffusion. This conclusion is supported by recent studies performed by Magnien et al. [35] and Roskosz et al. [36] on the kinetics of iron redox reactions in silicate melts. Magnien et al. [35] have determined that at superliquidus temperatures, the diffusion of oxygen represents the dominant mechanism in the kinetic of iron redox reactions in silicate melts. Roskosz et al. [36] described a more complex mechanism where the rate-limiting step is either diffusion of oxygen in the volume, or incorporation of oxygen at the sample surface that limits the bulk oxidation state of the liquid.

- The existence of the pyroxene phase has been clearly evidenced in the soda-silicate melts with the lowest Na contents and for temperatures lower than 1160°C. By taking the existence of this phase into account, the morphology of corroded chromium or chromium-alloys by molten glasses may be better understood.

Acknowledgements : The authors gratefully acknowledge J. Ravaux for performing electron-probe micro-analyses ("Service Commun d'Analyses par Microsonde Electronique" of Nancy). This work was financially supported by the ANR through the Actimelt project.

REFERENCES

[1] C. Rapin, M. Vilasi, R. Podor, A. Carton, B. Gaillard-Allemand, P. Berthod, P. Steinmetz, Mater. Sci. Forum 461-464 (2004) 1125.

[2] H. Khedim, S. Abdelouhab, R. Podor, C. Rapin, M. Vilasi, Materials Sciences Forum, 595-598 (2008) 621.

[3] S. Abdelouhab, Détermination de grandeurs physicochimiques dans les verres fondus – Relation avec le comportement du chrome et d'alliages chromine-formeurs, PhD Thesis, Université Henri Poincaré, Nancy (2005).

[4] S. Abdelouhab, R. Podor, C. Rapin, M.J. Toplis, P. Berthod, M. Vilasi, J. Non-Cryst. Solids. 354 (2008) 3001.

[5] H. Khedim, R. Podor, C. Rapin, M. Vilasi, J. Am. Ceram. Soc. 91 (2008) 3571.

[6] H. Khedim, T. Katrina, R. Podor, P.-J. Panteix, C. Rapin, M. Vilasi, J. Am. Ceram. Soc. 93 (2010) 1347.

[7] H. Khedim, R.Podor, P.J. Panteix, C. Rapin, M.Vilasi - Solubility of chromium oxide in binary soda silicate melts – submitted in J. Non-Cryst. Solids. in October 2009.

[8] H.C. Graham, H.H. Davis, J. Am. Cera. Soc. 54 (1971) 89.

[9] J-Y. Tilquin, P. Duveiller, J. Glibert, P. Claes, J. Non-Cryst. Solids. 211 (1997) 95.

[10] P. Claes, Ph. Duveiller, J-Y. Tilquin, J. Glibert, Phys. Chem. 100 (1996) 1479.

[11] D. Caplan, M. Cohen, J. Electrochem. Soc. 108 (1961) 1005.

[12] R. Mathieu, H. Khedim, G. Libourel, R. Podor, L. Tissandier, E. Deloule, F. Faure, C. Rapin, M. Vilasi, J. Non-Cryst. Solids. 354 (2008) 5079.

[13] Software Analysis, Soft Imaging System Gmbh

[14] H.F. Shermer, J. Res. Nat. Bur. Stand. 57 (1956) 97.

[15] CRC Materials Science and Engineering Handbook 50

[16] A. Tsuchiyama, H. Nagahara, I. Kushiro, Geochim. Cosmochim. Acta. 45 (1981) 1357.

[17] Y. Yu, R.H. Hervins, C.M. O'D Alexander, J. Wang, Geochim. Cosmochim. Acta. 67 (2003) 773.

[18] C. A. Stearns, R. A. Miller, F. J. Kohl, G. C. Fryburg, J. Electrochem. Soc. 124 (1977) 1145.

[19] Yan Liang, Frank M. Richter, Andrew M. Davis, E. Bruce Watson, Geochim. Cosmochim. Acta. 60 (1996) 4353.

[20] J.F. Stebbins , S. Sen, A.M. George, J. Non-Cryst. Solids. 192& 193 (1995) 298.

[21] M.J. Toplis, Chem. Geol. 174 (2001) 321.

[22] J.P. Pool, Verres Réfract. 2 (1948) 222

[23] R. Knoche, D.B. Dingwell, F.A. Seifert, S.L. Webb, Chem. Mineral. 19 (1994) 381

[24] R.J. Kirkpatrick, L.C. Kuo, J. Melchior, Am. Mineral. 66 (1981) 223.

[25] A. Tsuchiyama, Am. Mineral. 68 (1983) 687.

[26] R.J. Kirkpatrick, G.R. Robinson, J.F. Hays, J. Geophys. Res. 81 (1976) 5715.

[27] A. Kouchi, Y. Sugawara, K. Kashima, I. Sunagawa, Contrib. Mineral. Petrol. 83 (1983) 177.

[28] F. Faure, N. Arndt, G. Libourel, J. Petrol. 47 (2006) 1591.

[29] R. Hill, P.L. Roeder, J. Geol., 82 (1974) 709.

[30] C. Maurel, P. Maurel, Bull. Mineral., 105 (1982) 640.

[31] P.L. Roeder, I. Reynolds, J. Petrol. 32 (1991) 909.

[32] A.A. Poustovetov, P.L. Roeder, Can. Mineral. 39 (2001) 309.

[33] J. Di- Martino, C. Rapin, P. Berthod, R. Podor, P. Steinmetz, Corros. Sci. 46 (2004) 1865.

[34] S. Abdelouhab, C. Rapin, R. Podor, P. Berthod, M. Vilasi, J. Electrochem. Soc. 154 (2007) C500.

[35] V. Magnien, D.R. Neuville L. Cormier, J. Roux, J.-L. Hazemann, D. de Ligny, S. Pascarelli, I. Vickridge, O. Pinet, P. Richet, Geochim. Cosmochim. Acta. 72 (2008) 2157.

[36] M. Roskosz, M.J. Toplis, D.R. Neuville, B.O. Mysen, Am. Mineral. 93 (2008) 1749.

Table 1 : Glass Compositions expressed in atomic%. EPMA = Electron Probe Micro Analyses ; CA = Chemical Analyses

Glass formulae	**Theoretical Na_2O**	**Theoretical SiO_2**	**Na_2O (EPMA)**	**SiO_2 (EPMA)**	**Na_2O (CA)**	**SiO_2 (CA)**
Na_2O-1.5SiO_2	40.00	60.00	39.08 (0.25)	58.25 (0.92)	39.45 (0.19)	59.09 (0.52)
Na_2O-2SiO_2	33.33	66.67	32.20 (0.46)	66.73 (0.39)	33.07 (0.22)	65.59 (0.61)
Na_2O-2.5SiO_2	28.57	71.43	28.83 (0.52)	71.17 (0.22)	-	-
Na_2O-3SiO_2	25.00	75.00	24.21 (0.14)	77.44 (0.69)	-	-
Na_2O-3.5SiO_2	22.22	77.78	21.44 (0.66)	77.16 (0.89)	22.38 (0.28)	76.78 (0.49)
Na_2O-4SiO_2	20.00	80.00	20.09 (0.09)	81.73 (0.58)	-	-

Table 2. EPM Analyses of a $Na_2O - 2SiO_2$ glass doped with 1 wt% Cr_2O_3 using two different electron beam conditions (*average values and standard deviations calculated from 50 analyses).

	Program P1	Program P2
Accelerating voltage (kV)	10kV	25kV
Beam current (nA)	5	10
Spot size diameter (μm)	5	12
Counting time on peak for Na (s)	6	6
Counting time on background for Na (s)	3	3
Counting time on peak for Si (s)	10	10
Counting time on background for Si (s)	5	5
Counting time on peak for Cr (s)	30	30
Counting time on background for Cr (s)	15	15
At% (Na)*	19.27 ± 0.36	20.65 ± 0.19
At% (Si)*	23.44 ± 0.18	22.76 ± 0.10
At% (Cr)*	0.26 ± 0.03	0.250 ± 0.01
Wt%(Na_2O)*	28.89 ± 0.58	31.39 ± 0.31
Wt%(SiO_2)*	68.14 ± 0.82	67.09 ± 0.62
Wt%(Cr_2O_3)*	0.97 ± 0.09	0.93 ± 0.04

Table 3: Volatilisation rates of dissolved Cr^{VI} species in Na_2O-$2SiO_2$ (+ 0.93% Cr_2O_3) at different temperatures

Temperature (°C)	**993**	**1107**	**1207**	**1310**
Volatilisation rate of dissolved Cr^{VI} (Cr_2O_3 wt% / s)*10^5	-1.52 (0.70)	-4.48 (1.44)	-5.80 (1.11)	-13.43 (2.73)

Figure 1: Schematic representation of the equilibria involved in the dissolution of Cr_2O_3 crystals in glass melts.

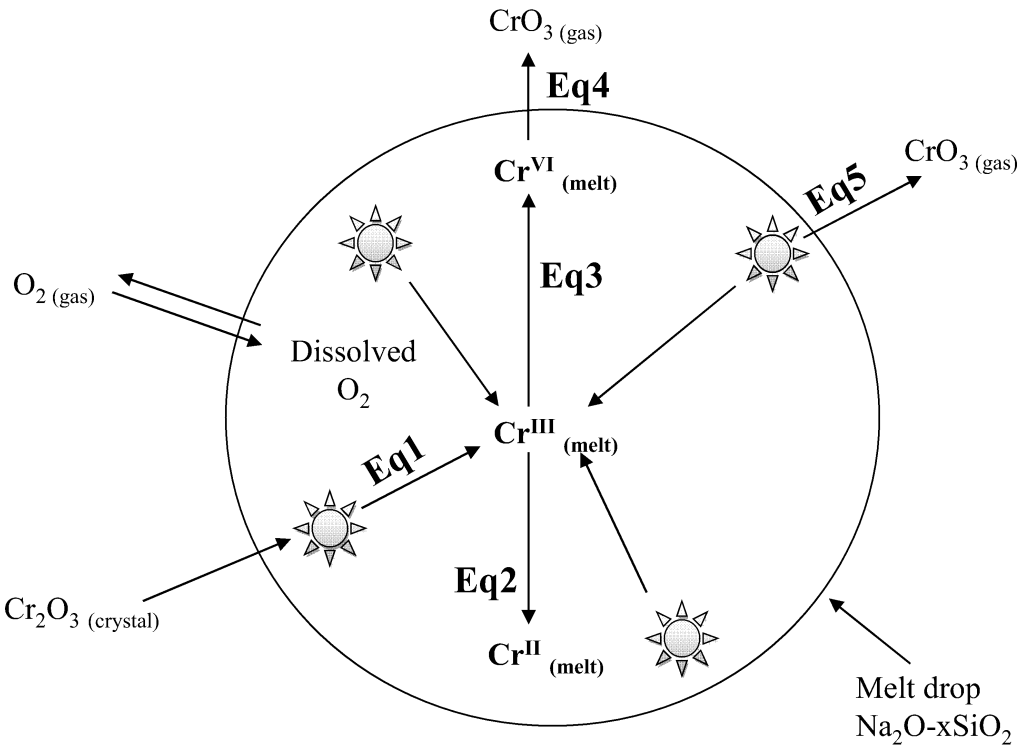

Figure 2: Distribution of the EPM analyses of a $Na_2O - 2SiO_2$ glass doped with 1 wt% Cr_2O_3 using two different electron beam conditions P1 (a) and P2 (b) (*average values from 50 analyses).

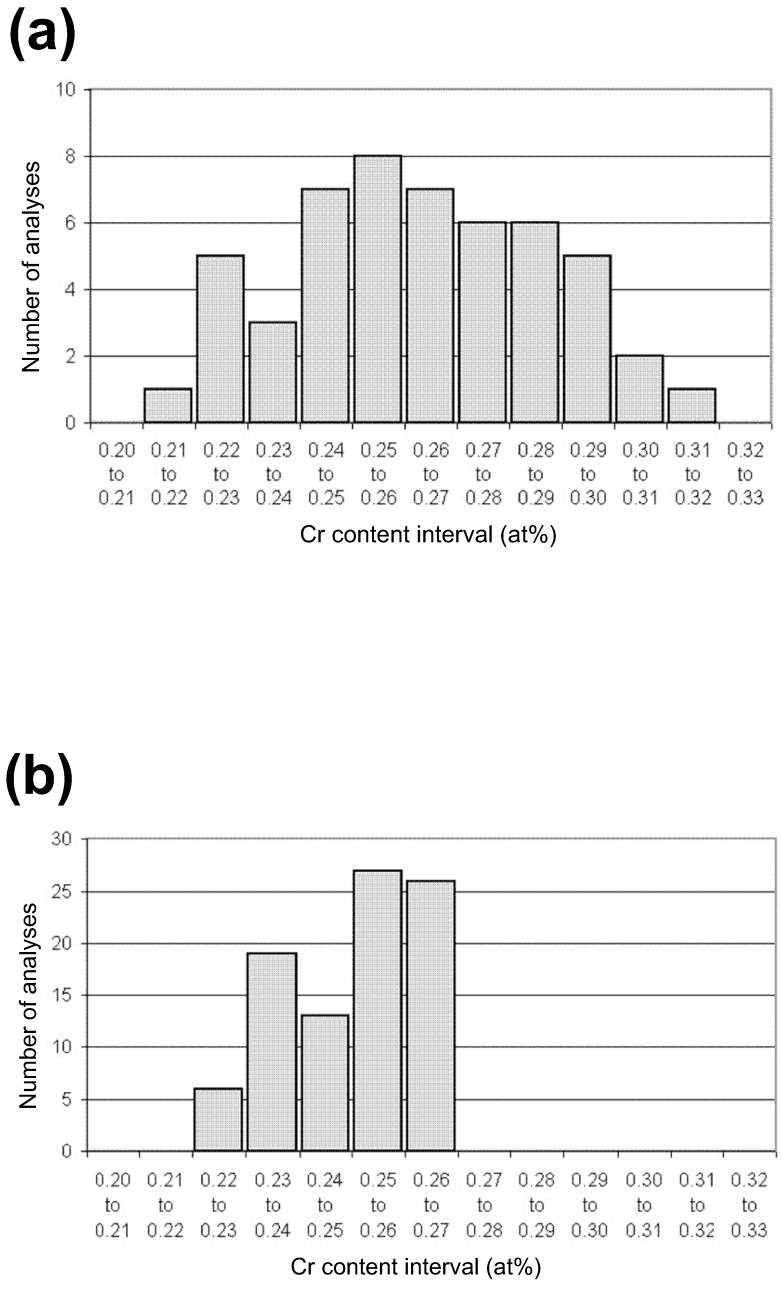

Figure 3: Variations of the Cr_2O_3 wt% dissolved in the initial Na_2O-$2SiO_2$ (+ 0.93% Cr_2O_3) melt reported as a function of run duration and temperature.

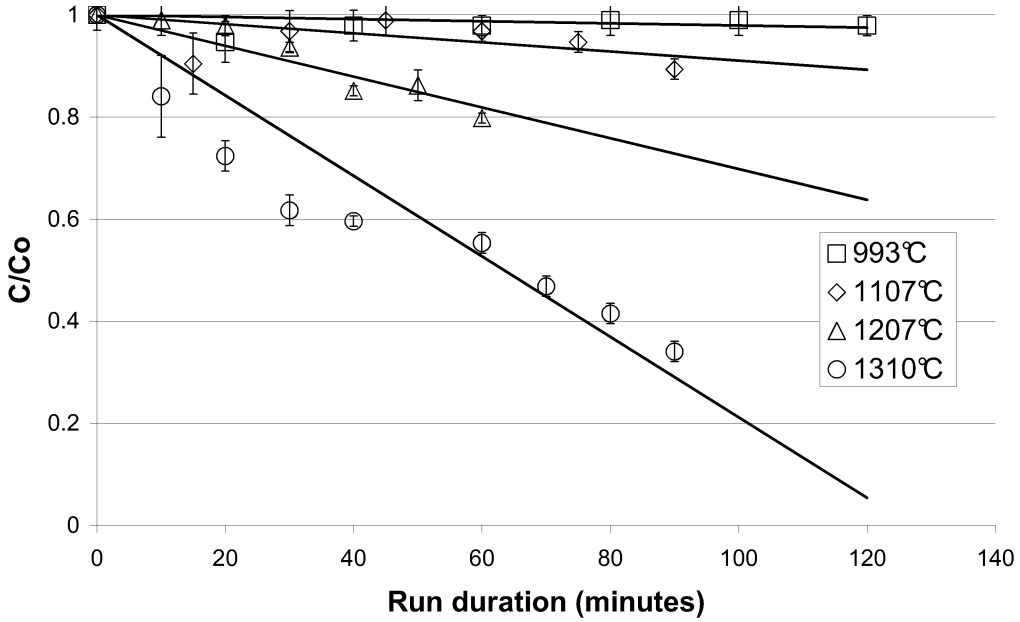

Figure 4: Plot of $\ln(V_R)$ versus 1/T in $Na_2O\text{-}2SiO_2$ (+ 0.93% Cr_2O_3).

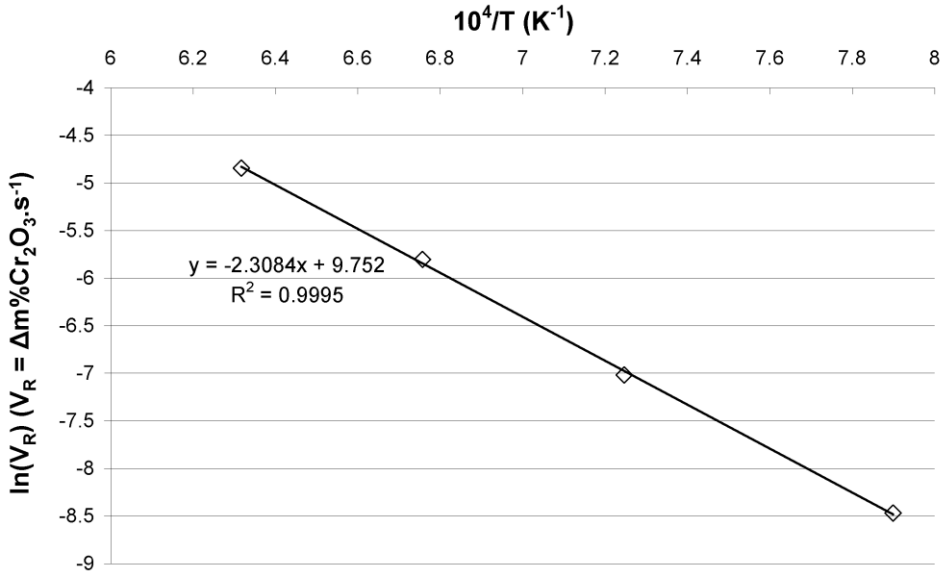

Figure 5: SEM observations on Na_2O-$2SiO_2$ drops containing 15 Cr_2O_3 wt% heat treated at T=1230°C for 10 minutes (a) and 30 minutes (b) in air.

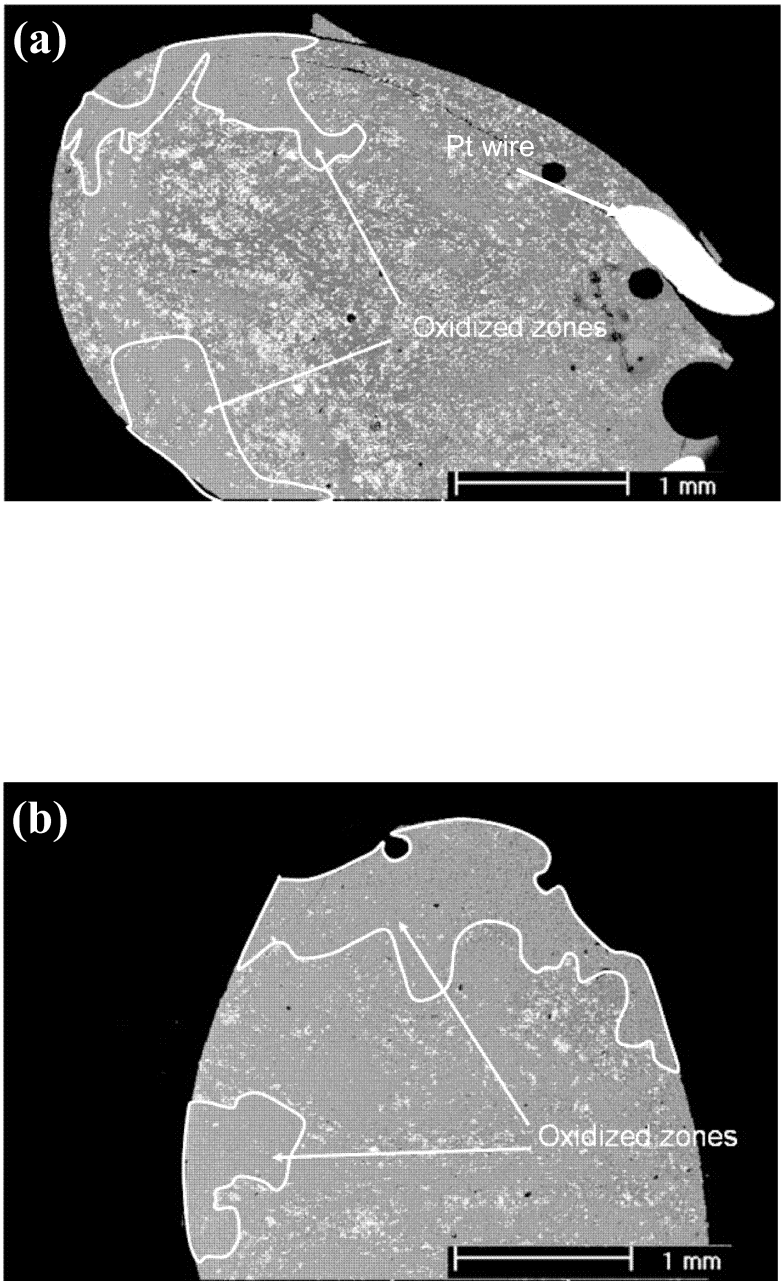

Figure 6: Dissolution kinetics of Cr_2O_3crystals at T=1230°C from supersaturated Na_2O-2SiO_2 (N2S) and Na_2O-4SiO_2 (N4S) melts.

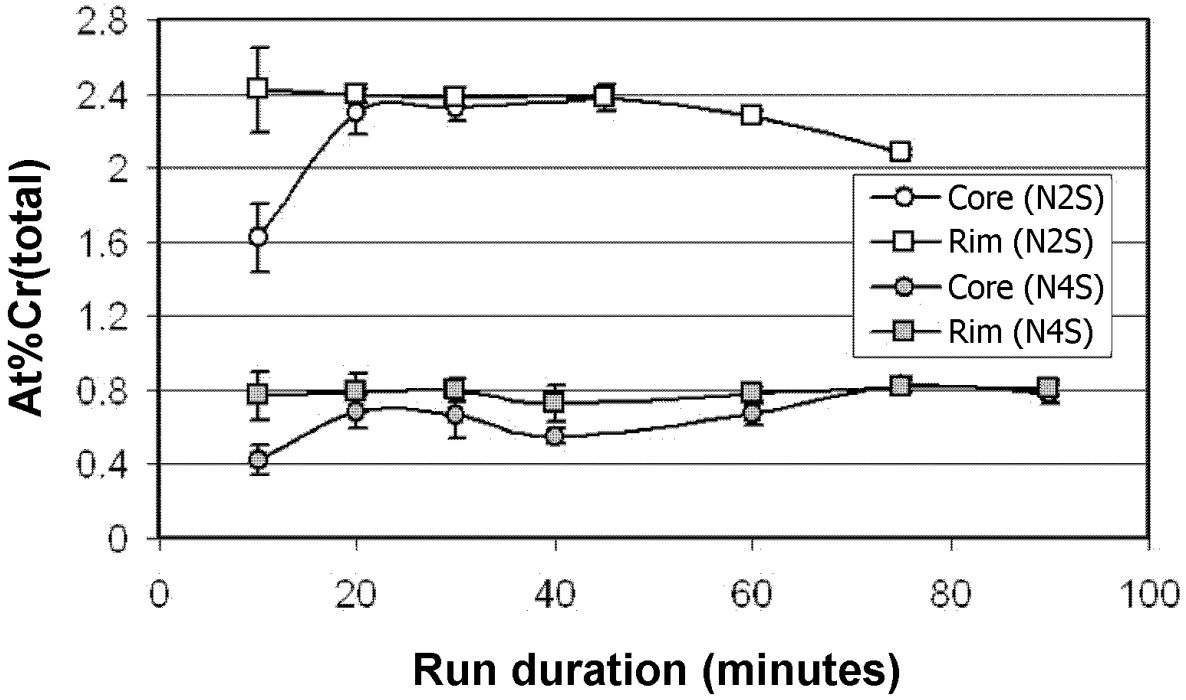

Figure 7: Time necessary to reach equilibrium reported as a function of melt viscosity (expressed in log η).

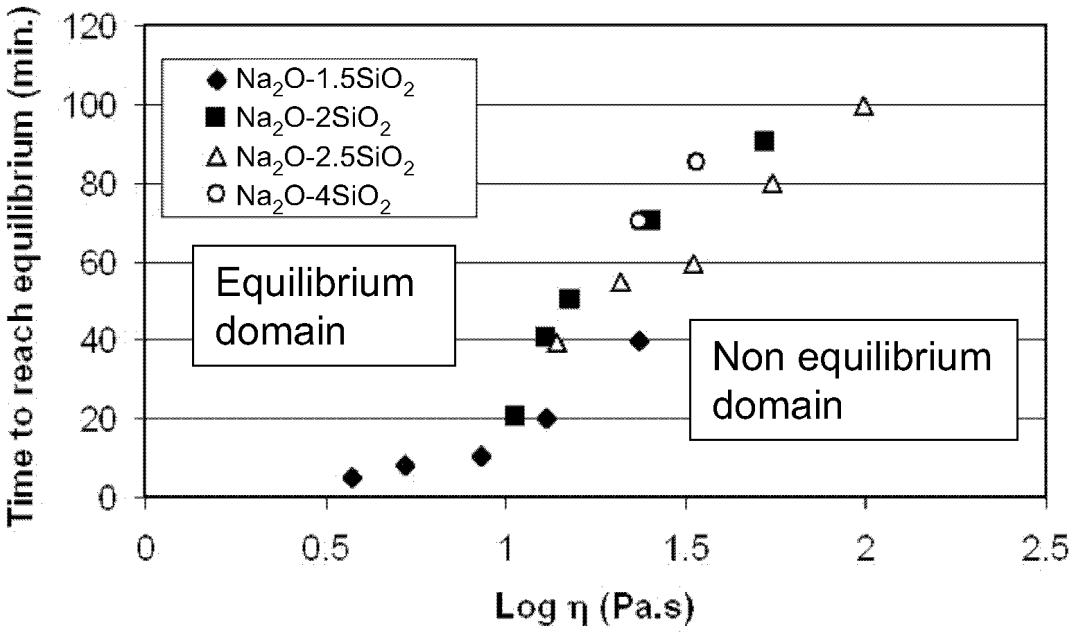

Figure 8: Equilibration of Cr_2O_3 with Na_2O-$3SiO_2$ soda-silicate melts at T=1200°C (T>1160°C domain), $fO_2=1.3\cdot10^{-11}$ atm (Fe/FeO buffer) (a). Corresponding melt features showing the Cr_2O_3 to $NaCrSi_2O_6$ transformation are reported (b).

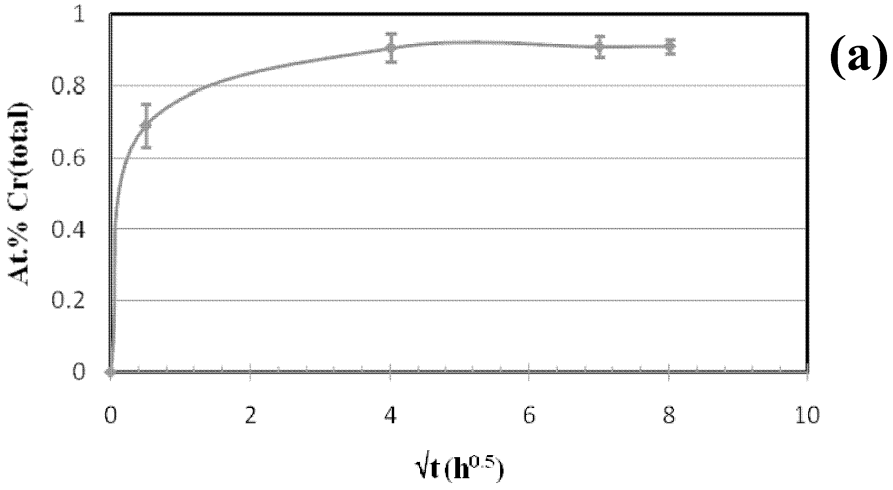

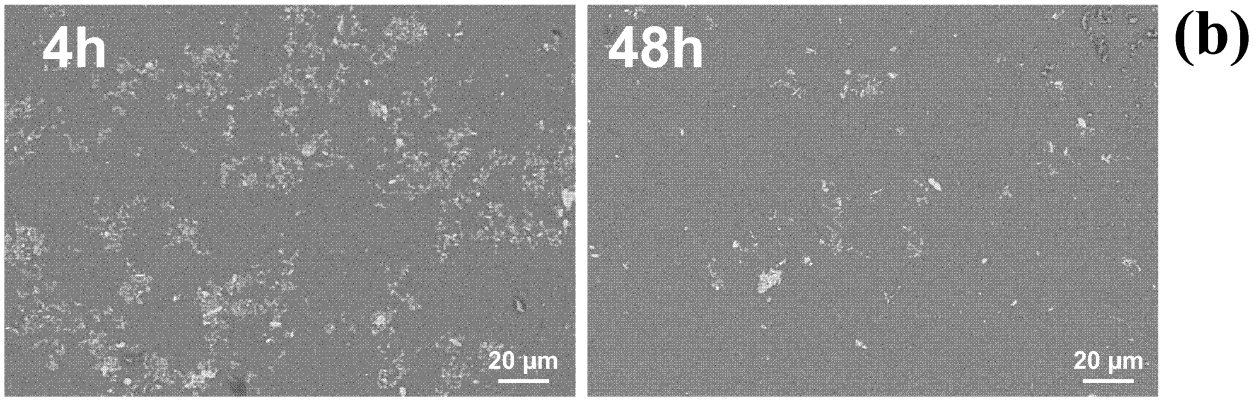

Figure 9: Kinetics of dissolution of chromium oxide in Na_2O-$2SiO_2$ at T=1150°C, fO_2=2.3.10^{-8} bars (Ni/NiO buffer)

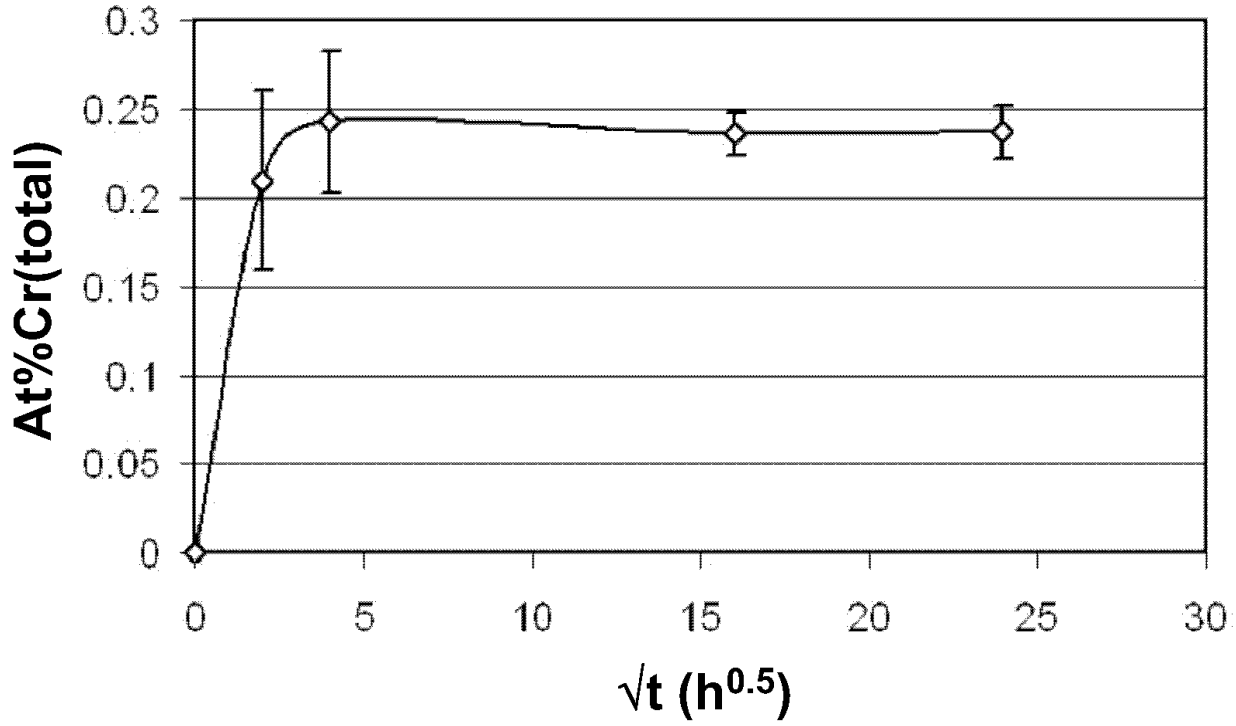

Figure 10: Dissolution kinetics of Cr_2O_3 in a Na_2O-3SiO_2 melt, T=1100°C, Ni/NiO fO_2 buffer (a). Corresponding melt features showing the Cr_2O_3 to $NaCrSi_2O_6$ transformation (b).

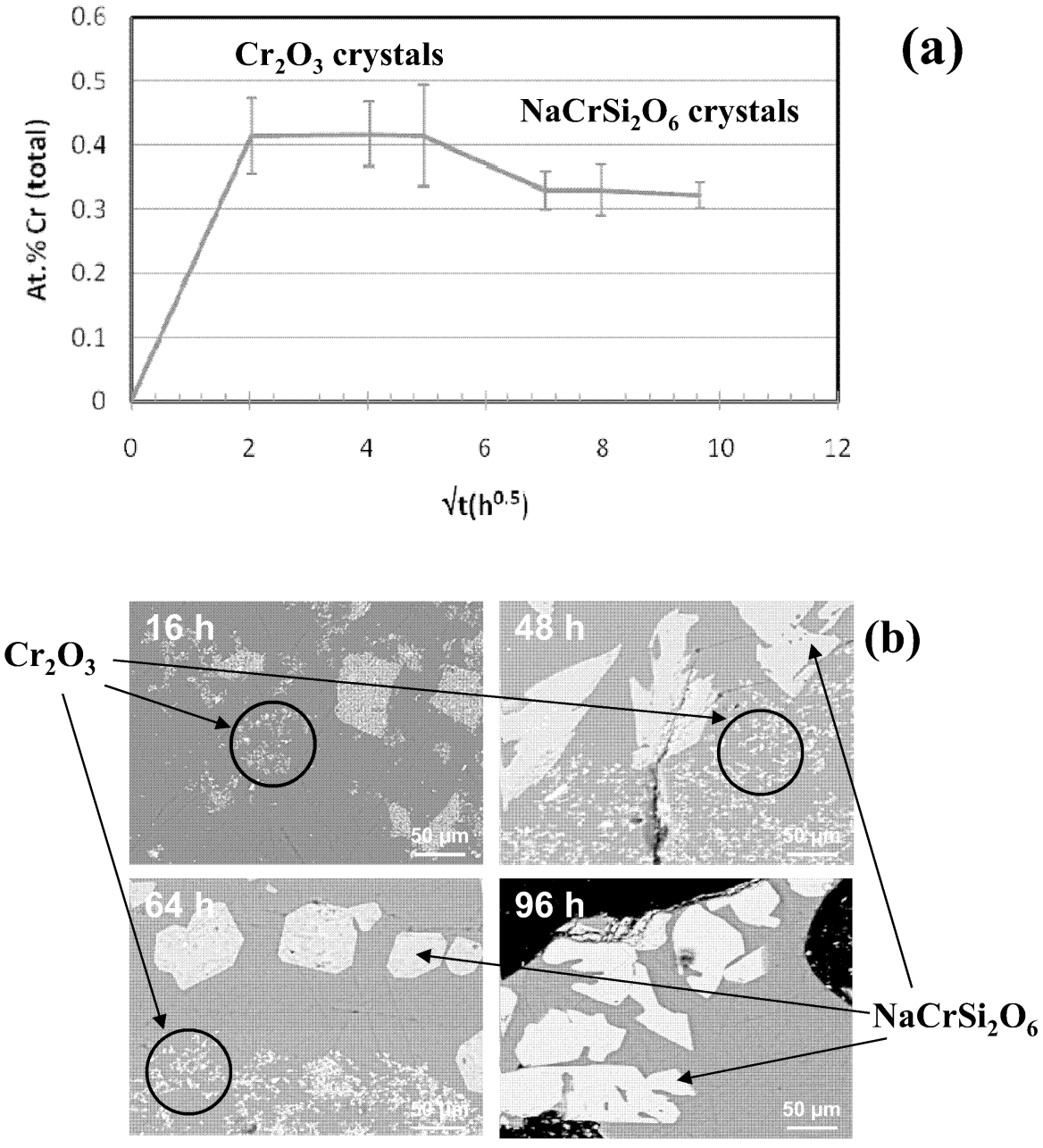

Figure 11: Dissolution kinetics of Cr_2O_3 in a Na_2O-3.25SiO_2 melt, T=1150°C, Ni/NiO fO_2 buffer.

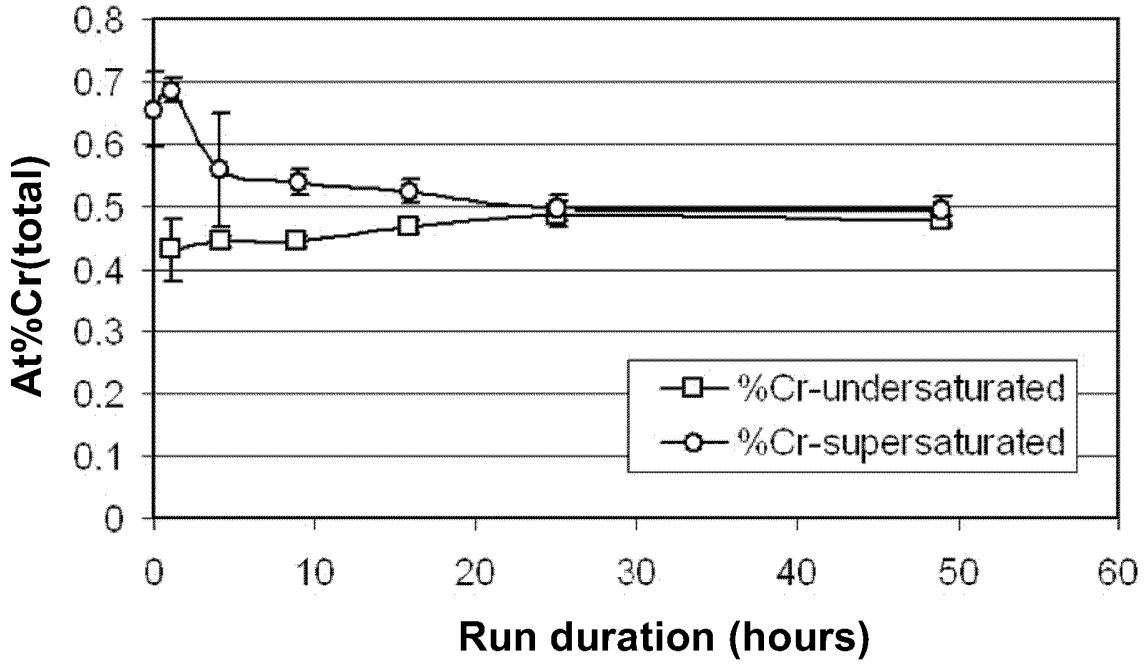

Figure 12: Arrhenius plot of Cr solubility in Na_2O-3.25SiO_2 melts in the studied temperature domain. The ○ point corresponds to the pseudo-equilibrium dissolution of Cr_2O_3 when T>1160°C.

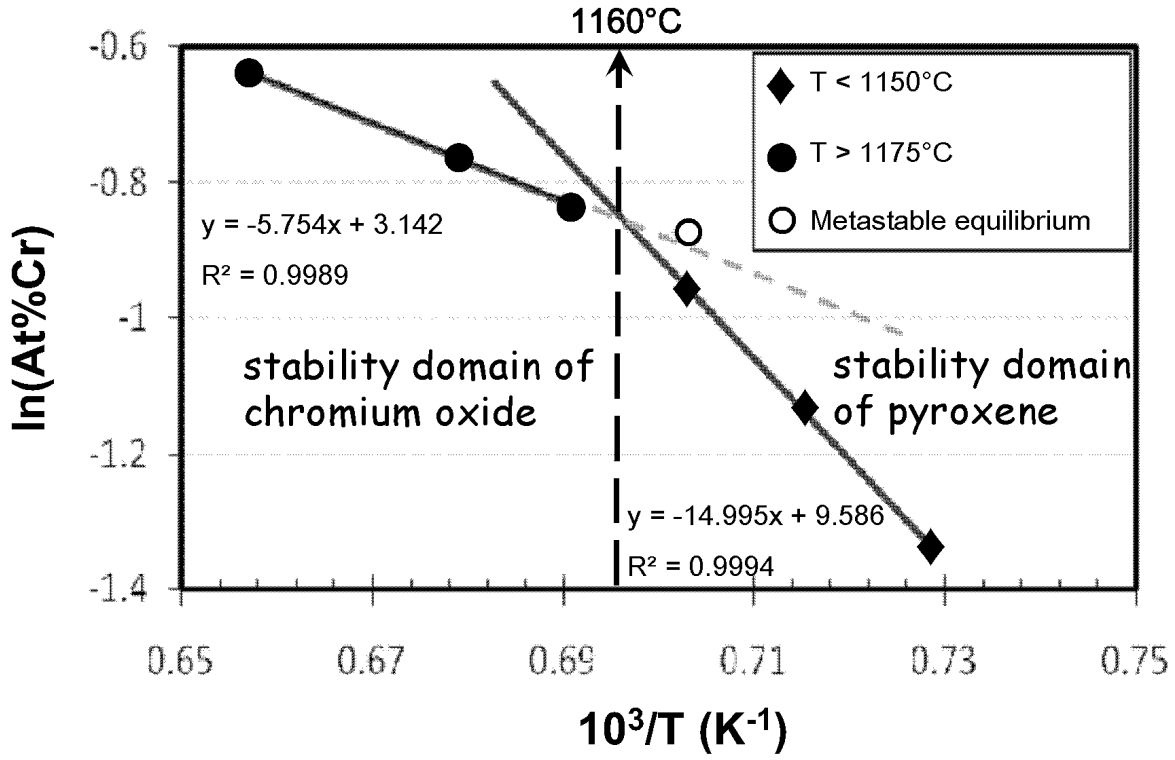

Figure 13: Morphology of Cr_2O_3 crystals precipated from a Cr^{VI}-containing Na_2O-$2SiO_2$ melt obtained by fast fO_2 decrease (T=1200°C).

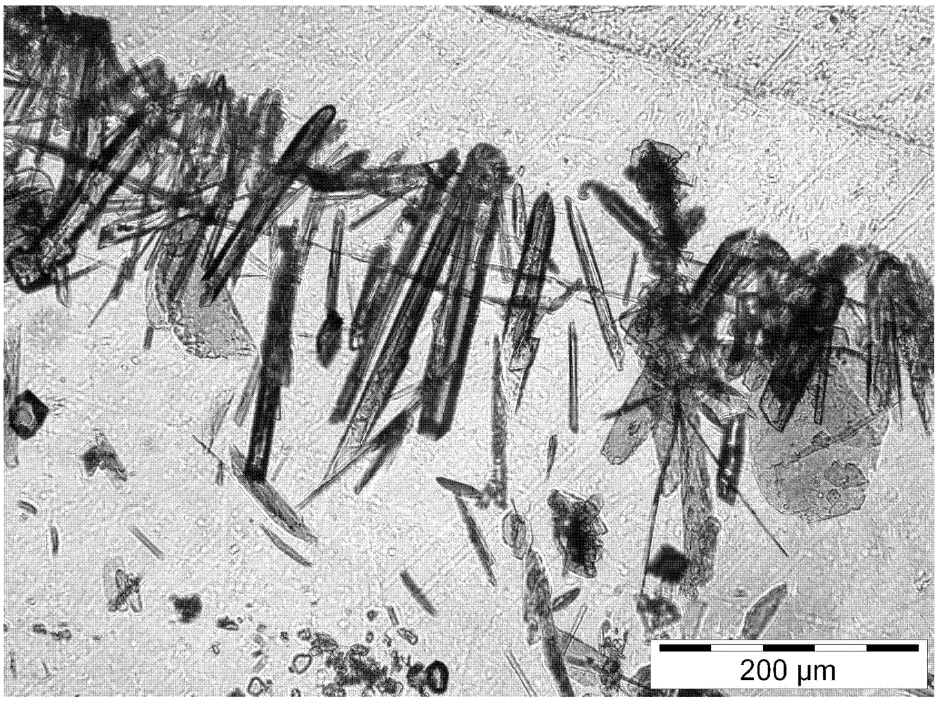

Figure 14: Typical morphology of Cr_2O_3 nodules crystallised in N3.25S glass, T=1150°C, Ni/NiO (a), density of germs (b), and Cr_2O_3 crystals length (c) vs heat treatment duration.

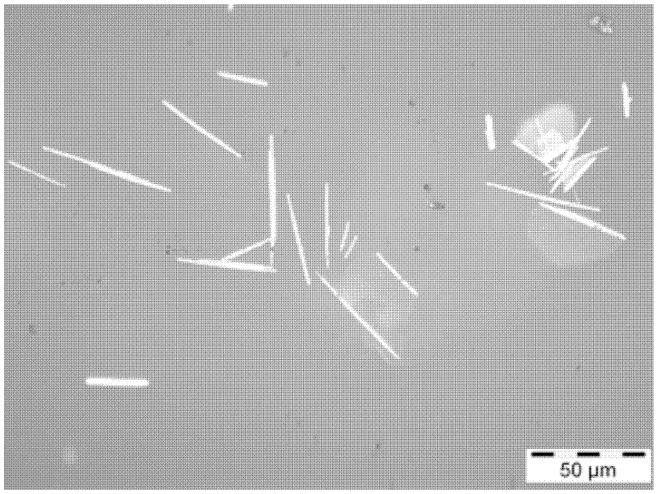

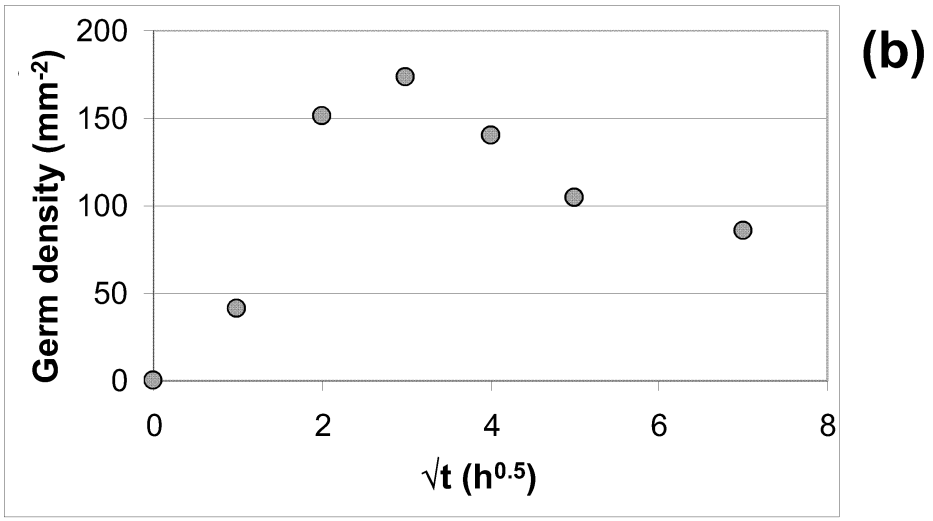

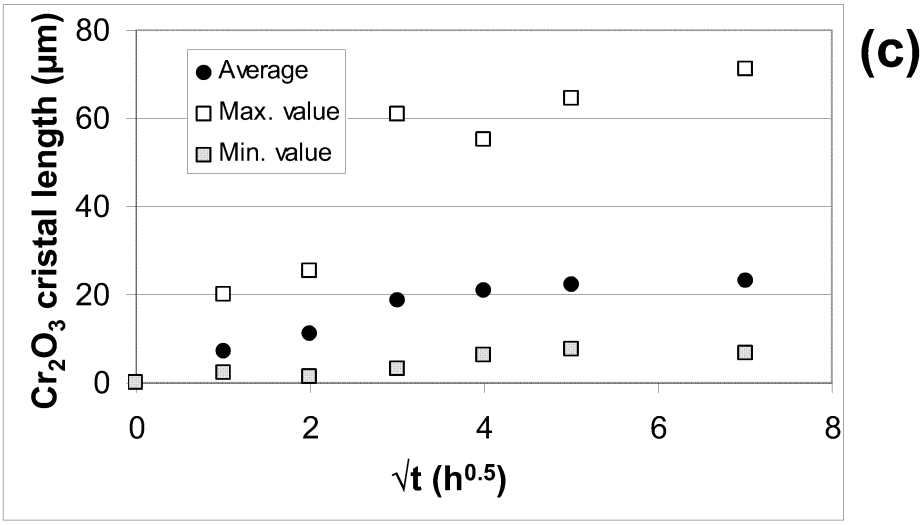

Figure 15: Typical morphology of pyroxene nodules crystallised in N3.25S glass, T=1150°C, Ni/NiO (a), pyroxene perimeter (b), and pyroxene surface (c) vs heat treatment duration.

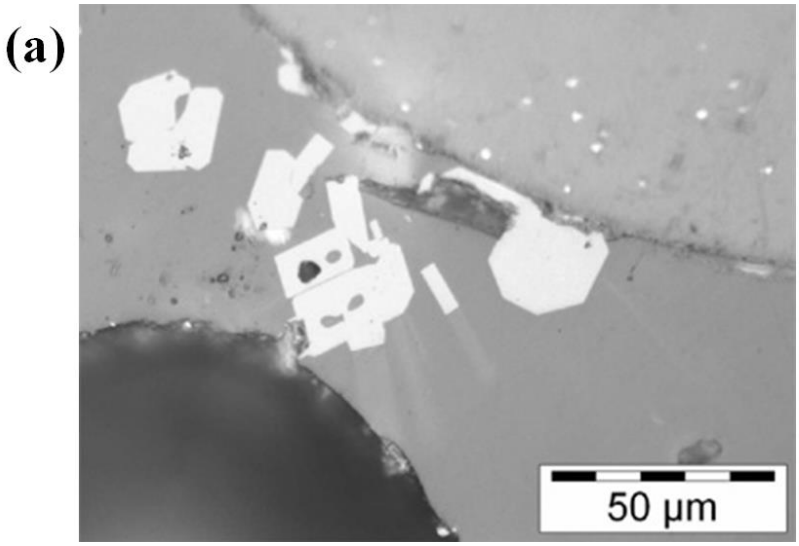

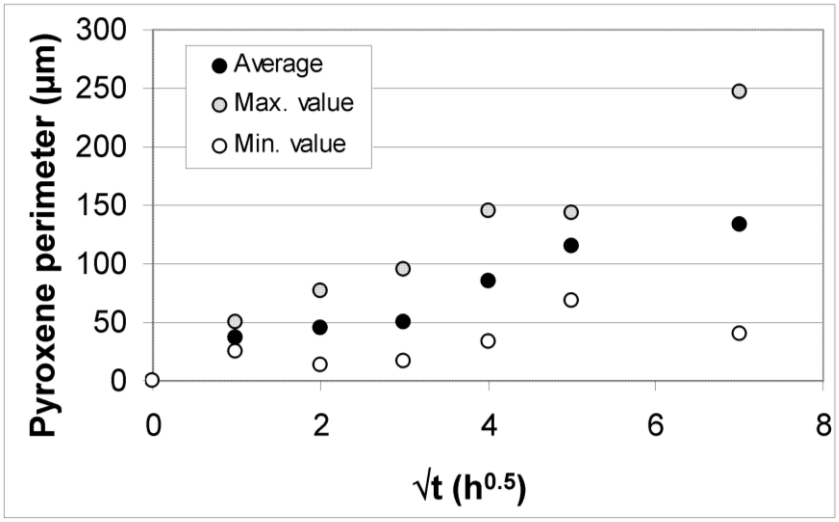

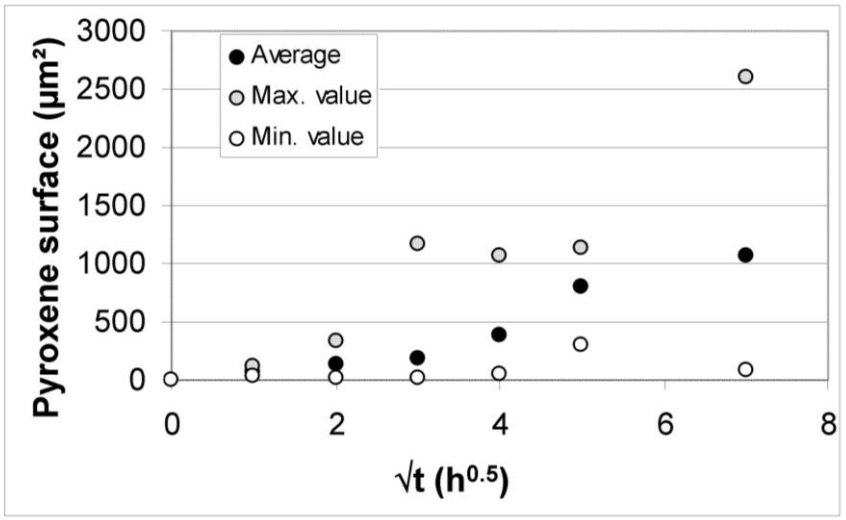

Figure 16: Representation of the stability domains of the different phases that are in equilibrium with the soda-silicate melts, as a function of melt composition, temperature and oxygen fugacity.

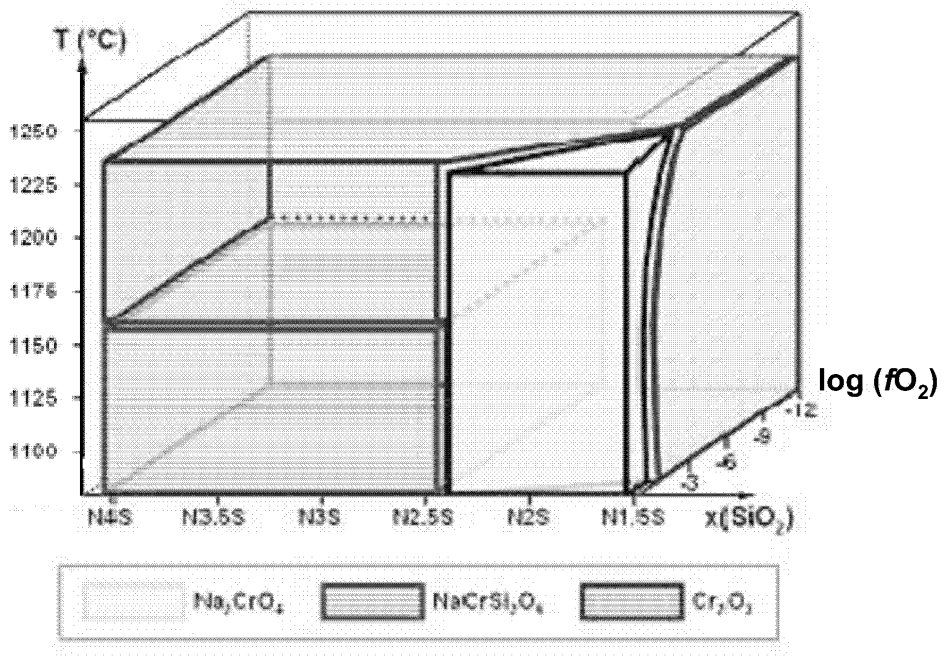

Figure 17: Na_2O-SiO_2-Cr_2O_3 phase diagrams under reducing conditions at T<1160°C.

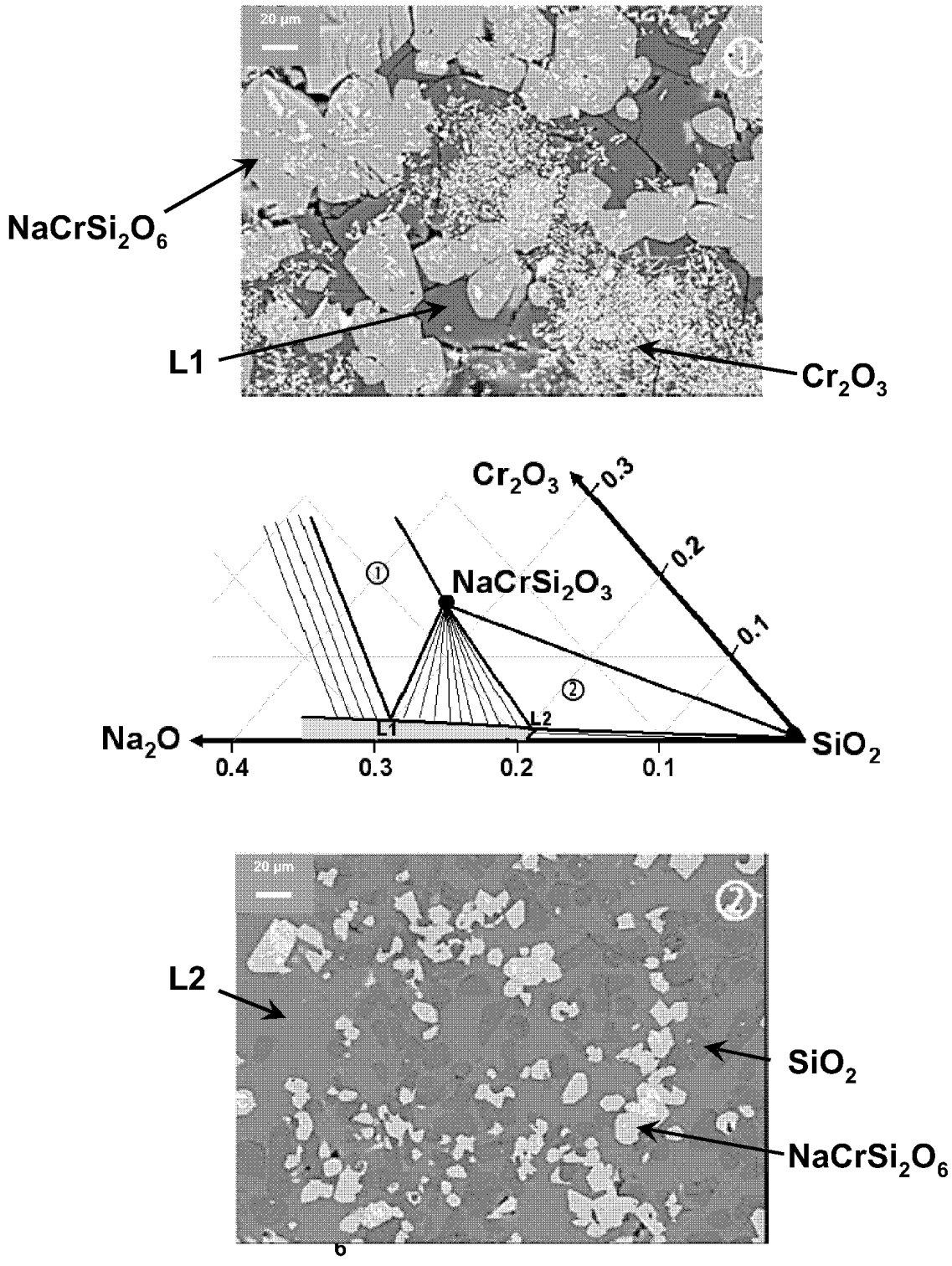

Figure 18: Na_2O-SiO_2-Cr_2O_3 phase diagrams under reducing conditions at T>1160°C.